Available online at www.sciencedirect.com
ScienceDirect
Journal of the European Ceramic Society 29 (2009) 1493–1499
www.elsevier.com/locate/jeurceramsoc

Pressureless reactive sintering of ZrB_2 ceramic

M. Brochu [a,*], B.D. Gauntt [b], L. Boyer [a,b], R.E. Loehman [b]

[a] McGill University, Mining and Materials Engineering, 3610 University, Montreal, Quebec, Canada H3A 2B2
[b] Sandia National Laboratories, Advanced Material Laboratories, 1001 University SE, Albuquerque, NM 87106, USA

Received 14 December 2007; received in revised form 19 August 2008; accepted 24 August 2008
Available online 15 October 2008

Abstract

Pressureless reactive sintering was investigated to fabricate ZrB_2 from a mixture of elemental Zr and B powders. Both hand mixing and high-energy milling were used to blend the powders. The sintering experiments were carried out at 1800, 2000 and 2200 °C. The samples made from the high-energy milled powders had relative densities varying between 66 and 79%, while the relative densities of the hand mixed powders varied between 58 and 70%. The average grain size of the sintered ceramic was independent of the mixing procedure and increased with the sintering temperature (from 8.5 to 23.5 μm for the hand mixed samples and from 4.6 to 34.9 μm for the milled samples).

Keywords: Powders—solid-state reaction; Milling; Sintering; Borides; ZrB_2

1. Introduction

The high-melting temperature of zirconium diboride (ZrB_2 $T_m > 3000$ °C) and improvements in ceramic processing have revived interest in ultra-high-temperature ceramics (UHTCs) for numerous severe applications. The highly covalent nature of bondings of these ceramics results in superior mechanical properties (hardness and strength) and oxidation resistance.[1–4] In particular, oxidation studies of several refractory diboride systems were conducted in the past[5] and Zr- and Hf-based systems were found to possess superior high-temperature oxidation resistance due to their high-melting point and low-vapor pressure of oxides and sub-oxides.[2–7] The improvement in properties is making these ceramics suitable for use in thermal protection systems for hypersonic flight, atmospheric reentry, and rocket propulsion systems.[1,2,8]

The high-melting temperature and apparent low-diffusion rates of ZrB_2 limit the applicability of conventional pressureless sintering processes.[9] Major successes in consolidating ZrB_2 have been obtained with pressure-assisted processes. For instance, hot pressing with various metallic, ceramic, or glass additives was previously used to make samples with nearly full density. However, the presence of a secondary phase limits the service conditions of the consolidated dense ceramic.[10–12] On the other hand, the fabrication of parts by hot pressing required substantial diamond machining. Such expensive processing has prompted a search for advances in pressureless sintering. Despite the low-intrinsic sinterability, which is attributed to highly covalent bonds and low volume and grain boundary diffusion rates,[13] significant advances in pressureless sintering have been made. Fahrenholtz and Hilmas fabricated pure ZrB_2 samples with relative densities of 98% using pressureless sintering of attrition milled powders[14] with sintering temperatures >2150 °C and soaking time of 540 min. Some applications for thermal protection systems may not require the very high-mechanical strengths of fully dense materials. Lower cost processing techniques that can produce large parts in complex shapes with some porosity may find application for thermal protection, as long as the material meets some threshold strength criterion for the particular design. The material porosity may even provide some benefit by lowering the stiffness and the thermal conductivity of the part.

Pressureless reactive processing (PRP) offers the possibility of reduced processing times and temperatures and is therefore an attractive alternative to conventional pressureless sintering of ZrB_2 powders. Reactive processing (RP) possesses advantages, such as lower processing temperatures, improvement in the cleanness of the grain boundaries and the usage of more readily available and less expensive precursors.[15] This

* Corresponding author. Tel.: +1 514 398 2354; fax: +1 514 398 4492.
E-mail address: mathieu.brochu@mcgill.ca (M. Brochu).

0955-2219/$ – see front matter © 2008 Elsevier Ltd. All rights reserved.
doi:10.1016/j.jeurceramsoc.2008.08.032

Table 1
Characteristics of the raw materials used

Powder	Vendor	Particle diameter distribution	Purity
Zr	Alfa Aesar	−325 mesh	98.5% Zr + 2% Hf
B (crystalline)	Alfa Aesar	−325 mesh	99%
ZrB_2	Cera	−325 mesh (APS 10 μm)	99.5%

processing route requires thermodynamically favorable reactions. The Gibbs free energy of reaction between Zr and B to form ZrB_2 is −306 kJ/mol at 727 °C and −280 kJ/mol at 1727 °C,[3] confirming the possibility of using RP for the formation of bulk ZrB_2. Reactive hot pressing has been reported for the Zr–B,[16] and Hf–B–SiC[17] systems. In all cases, near fully dense ceramic samples were produced with mechanical and oxidation properties similar to samples consolidated by other methods. Research targeting the control of grain size during reactive hot pressing by controlling the particle size distribution of the precursors is currently under way.[15]

The objective of this work was to study for the first time, the processing of ZrB_2 ceramic using pressureless reactive sintering of Zr and B elemental powders in order to investigate if this processing route could overcome the known difficulties of directly pressureless sintering ZrB_2 powders. Conventional sintering cycles were used with ZrB_2 powders to compare the reactive and non-reactive pressureless sintering processes. This work emphasizes the identification of thermal events during sintering, densification behavior, and phase and microstructure evolution.

2. Experimental procedures

Commercially available powders were used, and some of their respective characteristics are presented in Table 1.

For reactive sintering, the powders were weighed to give stoichiometric ZrB_2. Two procedures were used to mix the elemental powders. In the first method, an isopropanol-based slurry containing the respective powders was hand-mixed using a agate mortar and pestle. This simple method was selected as it is believed to minimize the loss of powder during the process. In the second method the powders were milled for 1 h in a Spex Certiprep Model 8000 mixer/mill with a powder-to-ball weight ratio of 10:1. A stainless steel vial and balls were used in the mixer/mill. The powders were loaded in the vial under an Ar atmosphere to minimize oxidation during milling. In both cases, 2 g of powders were mixed at a time. The ZrB_2 powders were also attrition milled at 600 rpm for 1 h in methyl alcohol.

Two grams of each mixture were cold pressed in a 9.5 mm diameter steel die under a uniaxial pressure of 550 MPa followed by cold isostatic pressing under 206 MPa for 1 min. The samples were bagged in plastic prior to the CIP to avoid direct contact with the compressing liquid. Sintering was performed in a controlled atmosphere furnace equipped with tungsten heating elements. The heating rate was 20 °C/min up to a sintering temperature of 1800, 2000 or 2200 °C, held at temperature for 1 h and cooled to room temperature at 20 °C/min. Flowing argon (ultra-high-purity grade) was maintained during the cycle.

Densities were measured using the Archimedes method in accordance to the procedure described in ASMT C20 standard. The phase analysis was carried out on solid samples in a Philips PW1710 diffractometer (Cu Kα radiation) between 20° and 80° at 0.05°/step for 1 s dwell time. The ceramic conversion was analyzed using the ratio of intensity of the ZrB_2(1 0 1) peak to the Zr(1 0 1) peak. The measured ratio of intensity was compared to the ratio of intensity acquired for mixtures of Zr and ZrB_2 of known composition. A detailed description of the procedure can be found in Cullity.[18] The heat treatment for the conversion study was designed to mimic the sintering cycle. The samples were heated at 20 °C/min to the tested temperature and immediately cooled at 50 °C/min to minimize reaction during cooldown. X-ray photoelectron spectroscopy (XPS) analysis was performed using Kratos Ultra XPS, equipped with a monochromatic Al Kα X-ray source (1486.6 eV). Oxygen 1s, boron 1s and zirconium 3d binding energies were analyzed for phase identification. The XPS measurements were performed on the surface of bulk ceramic samples. Prior to examination, the surfaces impurities were removed using the in situ ion gun.

Cross-sections of selected samples were automatically polished down to 0.25 μm using an automated polishing machine (Buehler Ecomet 3®). The final polishing (0.02 μm colloidal silica) was performed on a Vibromet 2® for 2 h. The thermally etched cross-sections were examined with a JEOL-840 scanning electron microscope coupled with an EDAX™ EDS system. The samples were coated with gold–palladium prior to examination. Image analysis on a minimum of 200 grains randomly selected on a minimum of 20 locations across the samples was carried out using Clemex Vision PE 5.0 software. Vickers microhardness was determined using a Clark CEM microhardness indenter with a load of 490 mN. Reported values were obtained from an average of 10 indents.

3. Results and discussion

Fig. 1 presents the powder morphology of the starting (a) zirconium and (b) boron powders, respectively. As shown by the micrographs, the Zr powders possessed an irregular shape, while the B particles had an angular morphology. Fig. 1(c) depicts the particle size distribution for the elemental powders. The average particle size for Zr and B is 19 and 18 μm, respectively. The specific particle size distribution of the Zr powder was selected to reduce the pyrophoric character associated with finer Zr powders. The XRD pattern of the starting Zr powder was in agreement with ICDD #05-0665 with slight peak shifts towards lower angles, which is believed to be caused by the presence of Hf impurity in solid solution in Zr.

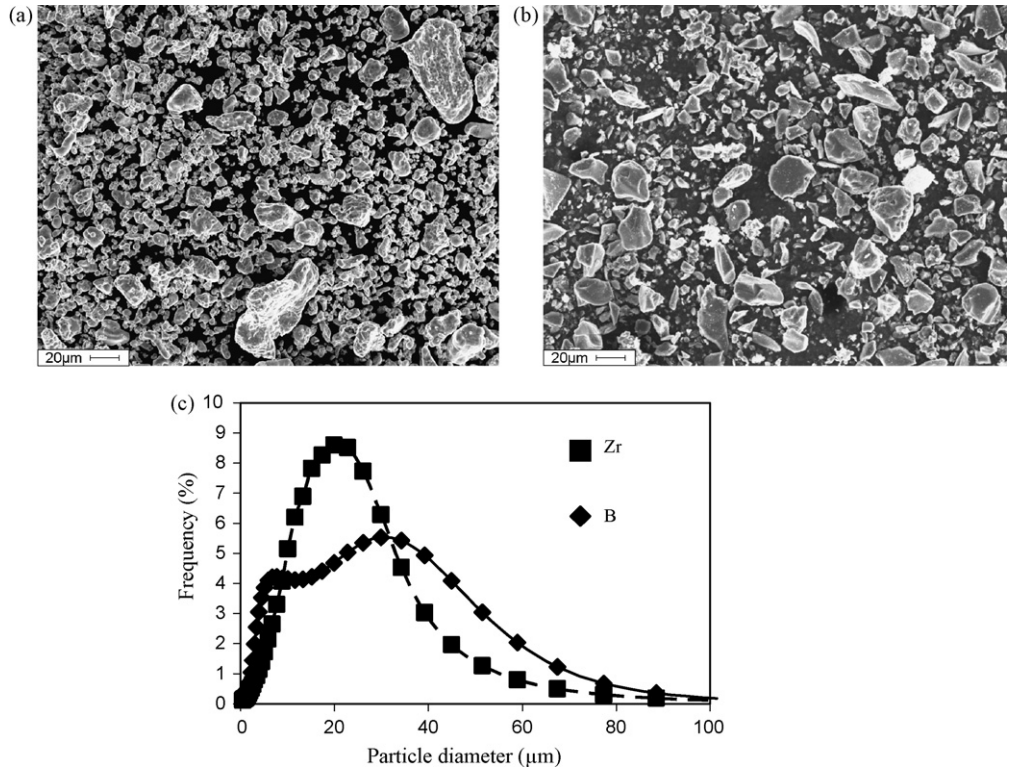

Fig. 1. Scanning electron micrographs of as-received (a) zirconium and (b) boron and (c) the respective particle size distributions.

No significant changes in morphology or particle size were observed by SEM after mixing the starting powders in the mortar and pestle. By contrast, the high-energy milling procedure produced Zr powder particles containing embedded boron. Fig. 2 shows cross-sections of particles blended for 1 h. As can be seen, the boron powders were fractured during the process and small fragments were embedded in the Zr matrix. It is worth mentioning that EDS analyses performed in numerous locations within the Zr matrix has not revealed the presence of Fe, indicating minimal contamination during milling. The microhardness of the Zr powders hand mixed in the mortar is 1.32 GPa, whereas the powders blended in the Spex mill had a microhardness of 10.56 GPa. The significant hardening of the latter Zr particles was caused by the presence of the embedded boron, which itself has a hardness of 48.05 GPa.[19]

X-ray diffraction analysis was used to determine the final ceramic conversion temperatures for both mixing procedures. Fig. 3 presents the evolution of ceramic conversion acquired through the ratio of the peak intensity from the XRD pattern for samples cooled down immediately after reaching the tested temperature, *i.e.*, without holding time at tested temperature followed by a cooling rate of 50 °C/min. As depicted, for the mortar mix, no significant reaction occurred below 1000 °C. The XRD pattern of the sample heat treated at 1600 °C and immediately cooled showed 64% conversion. Full conversion was obtained for the mortar mixed sample when the samples were either (1)

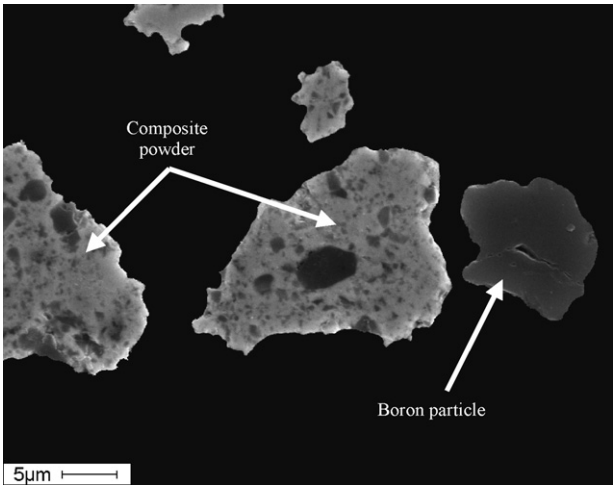

Fig. 2. Cross-section of composite powder after 1 h of milling.

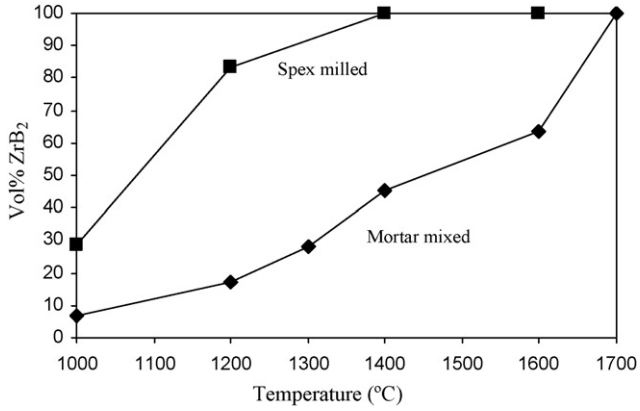

Fig. 3. Trend of ZrB_2 formation as a function of temperature, no additional isotherm hold.

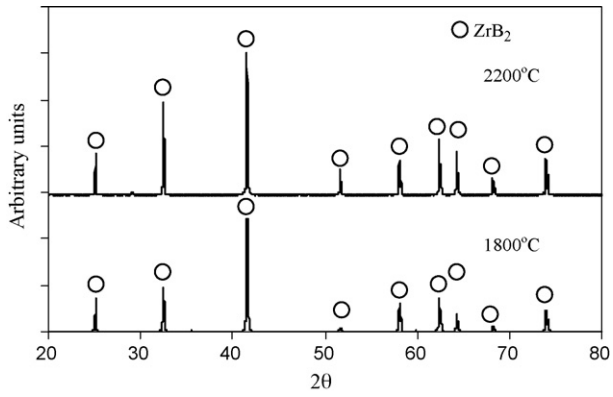

Fig. 4. X-ray diffraction pattern of Zr + B samples hand-mixed and sintered at 1800 and 2200 °C.

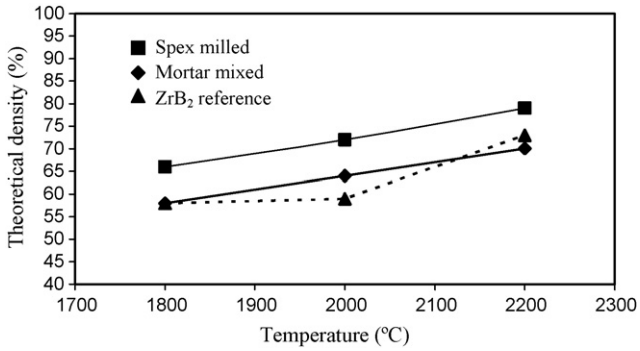

Fig. 5. Percentage of theoretical density of ZrB_2 ceramics after sintering.

heated at 1600 °C and soaked for 1 h or (2) heated to 1700 °C and immediately cooled.

The intimate powder mixture obtained using the Spex mill showed a significant difference in ceramic conversion behavior. As depicted in Fig. 3, full conversion was obtained by heating/cooling cycle at a temperature as low as 1400 °C. Thus, the homogeneous distribution of fine boron particles increases the number of sites for nucleation of ceramic grains during the conversion, reduces the diffusion distances, and favors conversion at lower temperature. Monteverde has performed similar analysis for pressureless synthesis of HfB_2-SiC composites from Hf, Si and B_4C, and reported that ceramic conversion is complete after a 1-h heat treatment at 1200 °C.[17] From our X-ray results, the conversion of the ceramic from both mixing procedures is expected to happen during the heating stage (1700 °C for hand mixed, 1400 °C for Spex milled powders) of the studied sintering cycle for UHTCs (from 1800 to 2200 °C). The high-temperature soak of the heat treatment would solely impact the densification of the ceramic compact.

After each sintering cycle the samples possessed the gray color characteristic of ZrB_2. Fig. 4 presents the X-ray diffraction patterns for the hand-mixed Zr and B mixture sintered at 1800 and 2200 °C. As expected, all samples contain only the ZrB_2 phase (agreement with ICDD #34-0423). Similar results were obtained for the samples reacted from the milled powders.

Fig. 5 presents the relative densities (%TD; based on the density of pure ZrB_2: 6.09 g/cm^3) of the different samples after various sintering cycles. For every mixing condition, the relative density increased with the sintering temperature. The reacted ZrB_2 composition from mortar-mixed elemental powders exhibited an increase in relative density from 58 to 64 to 70% for sintering cycles performed at 1800, 2000 and 2200 °C, respectively. The high-energy milled elemental powders showed an increase in relative density from 66 to 72 to 79% for the same sintering cycles. Thus, an improvement in density varying between 8 and 10% was obtained by mechanical mixing instead of simple hand mixing. In comparison, the samples made from ZrB_2 powders exhibited an increase in the theoretical density from 58 to 59 to 73%, which was a lower densification behavior than for the powders mixed in the Spex mill but similar to the hand mixture. In this case, no significant advantage, in terms of relative density, was found between sintering ZrB_2 powders and hand mixed Zr–B powder mixtures. Table 2 presents a comparison of relative densities with other work available in the literature. The results showed that for similar sintering temperatures, higher or similar relative densities were obtained for samples processed by pressureless reactive sintering compared to samples processed by pressureless sintered ZrB_2 powders, but with significantly shorter sintering times. As mentioned previously, Chamberlain et al.[14] have shown that extending the sintering parameters to 2150 °C for 9 h resulted in ZrB_2 samples with relative densities of 98%. Thus, we believe that nearly full density will be obtained if the sintering temperature is increased and the soaking period is extended.

Fig. 6 presents representative micrographs of the attrition milled mixture after the sintering cycle with 1 h at (a) 1800 °C and (b) 2200 °C, respectively. As depicted, the micrographs were in agreements with the relative density values presented in Fig. 5. Back-scattered micrographs and EDS analysis were used to verify the completion of the ceramic conversion and neither elemental Zr or B was observed in either microstructure as the conversion to ZrB_2 was completed before the soaking period. This observation is reinforced by the XRD results presented in Figs. 3 and 4. The EDS analysis showed peaks of Zr, B and a minor peak for Hf, which was an impurity in the starting Zr powder. In comparison, Fig. 7 presents micrographs of the directly

Table 2
Comparison of relative density of ZrB_2 processed by different routes

Fabrication route	Mixing process	Sintering parameters	Relative density (%)	Reference
Pressureless reactive sintering	Spex milled	2000 °C, 1 h	72	This work
Pressureless reactive sintering	Spex milled	2200 °C, 1 h	79	This work
Pressureless sintering ZrB_2	Attrition milling	2000 °C, 3 h	65	[11]
Pressureless sintering ZrB_2	Attrition milling	2150 °C, 3 h	72	[11]
Pressureless sintering ZrB_2	Attrition milling	2150 °C, 6 h	79	[11]

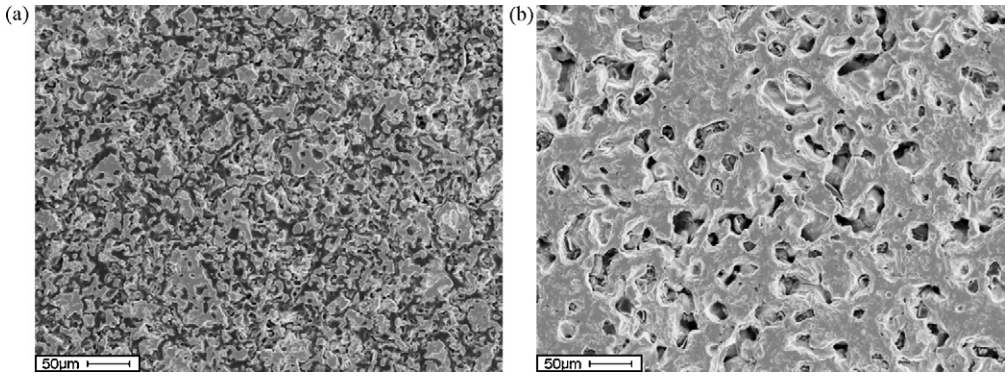

Fig. 6. Micrographs of ZrB_2 samples produced in the Spex mill and sintered for 1 h at (a) 1800 °C and (b) 2200 °C.

sintered ZrB_2 powders in which a different microstructure was observed. The ceramic samples produced from the mixture of elemental powders had a lower volume fraction of larger pores. The image analysis confirmed that the average pore diameter for the samples made from the blended, elemental powders was 27 ± 15 μm while the average pore size was smaller and narrower (6 ± 2 μm) for those specimens sintered from ZrB_2 powder.

The results on the relative densities after reaction and the micrographs of specimens after the various sintering cycles suggest a mechanism for pressureless reactive sintering. First, formation of ZrB_2 from a stoichiometric Zr and B powder mixture should itself give a 24% increase in density. Second, previous work on reactive hot pressing of ZrB_2 concluded that the B diffuses into the Zr phase to form the ceramic.[15,16] Although the detailed reaction mechanism for formation of ZrB_2 from the elements is not known, the hexagonal ZrB_2 unit cell is smaller than that of Zr (Zr: $a = 3.232$ Å, $c = 5.147$ Å from ICDD 05-0665; ZrB_2: $a = 3.169$ Å, $c = 3.530$ Å from ICDD 34-0423). The pores created from reaction in reactive hot pressing are closed by the applied pressure. In the present case of pressureless reactive sintering the pores can be eliminated only by normal sintering mechanisms, which as we have discussed, are slow for these covalently bonded borides. The smaller size, and homogeneous distribution of the B particles (see Fig. 2) as modified by the high-energy milling positively affect the final relative density of specimens in the present study. The driving force for pore shrinkage during sintering is reduction of the surface energy of the powder compact. Larger particles and pores have lower curvature and therefore lower surface energies. The pores created by the disappearance of large starting B particles (see Fig. 1(c)), as with the hand-mixed samples, were likely to have an insufficient driving force for densification, and combined with the absence of applied pressure, explain the low-final relative density. Alternatively, the pores created during the reaction of the powders subjected to high-energy milling were smaller and had a higher driving force for densification and pore shrinkage, which was reflected by the higher relative density.

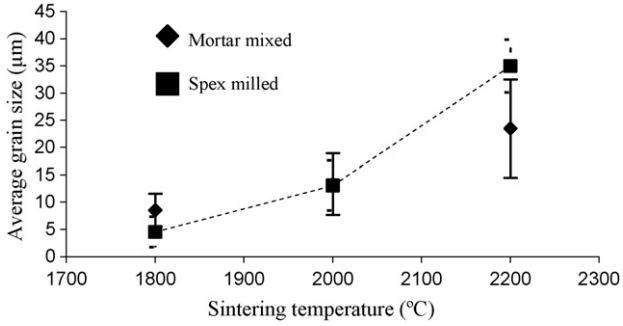

Fig. 8. Average grain size of the ZrB_2 samples after sintering cycle.

Fig. 8 presents the average grain size for the reactive sintered samples as a function of the sintering temperature. As observed, the average grain size increased with the sintering temperature and no significant grain size difference was observed between the two milling methods. The average grain

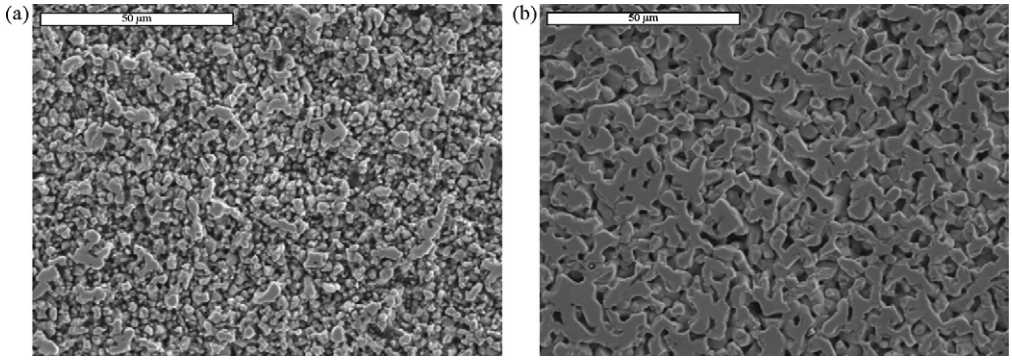

Fig. 7. Micrographs of ZrB_2 samples produced from ZrB_2 powders sintered for 1 h at (a) 1800 °C and (b) 2200 °C.

size increased from 8.5 ± 3.0 to 13.2 ± 5.7 to $23.5 \pm 9.0\,\mu m$ for the hand mixed samples while it increased from 4.6 ± 2.8 to 13.0 ± 4.6 to $34.9 \pm 4.9\,\mu m$ for the Spex-milled samples. Despite the improvement in relative density observed for the pressureless reactive sintered samples, the grain size was significantly larger than for the samples made by pressureless sintering of ZrB_2 powder, where an average grain size of $9.1\,\mu m$ was reported.[14]

Comparing the increase in specimen density and grain size at 2000 and 2200 °C, it is apparent that under our conditions ZrB_2 coarsens without major densification. Previous results on pressureless sintering of other boride ceramics (TiB_2 and B_4C) have shown the deleterious influence of oxygen contamination on the densification behavior, where with the increase in oxygen content, the densification rate decreased and significant grain growth occurred.[20,21] The presence of a B_2O_3 surface film was associated with the low-temperature coarsening of the microstructure in various boride ceramics.[14,20,21] Scarce literature is found regarding the boiling temperature of B_2O_3, which is reported to range between 1860 and 2065 °C.[21] Since the boiling point can be defined as the temperature where the vapor pressure of the liquid equals the total pressure of the surrounding atmosphere, the gas pressure maintained in the furnace during the heat treatment has a significant influence on the boiling temperature. Chamberlain et al.[14] presented the thermodynamic equilibrium vapor pressure of B_2O_3 as a function of temperature. From this relation, at atmospheric pressure, which was the pressure used in this work (flowing argon), the calculated boiling temperature is 2136 °C. Moreover, considering the current sintering parameters and conditions, and using the ZrB_2 volatility diagram reported by Fahrenholtz,[22] the coexistence of ZrO_2(s) and B_2O_3(l) is predicted. Lee and Speyer[21] suspected the presence of residual B_2O_3 liquid up to 2010 °C during sintering of B_4C under flowing He gas. They also reported that during the sintering of B_4C at a temperature of ~2140 °C, the relation between the sintering mechanism and grain coarsening was governed by the evaporation and condensation of B_4C, which is known to favor grain coarsening over densification.[21]

To better understand the impact of oxygen on the densification of ZrB_2 from elemental precursors, XPS was carried out on the as-received, milled powders and sintered samples: the results are presented in Fig. 9. Fig. 9(a) shows the binding energy of the as-received Zr powders. The measured binding energies of the Zr $3d_{3/2}$ and Zr $3d_{5/2}$ were respectively 184.5 and 182.1 eV, respectively, which is higher than the reference values for pure Zr (Zr $3d_{3/2}$: 181 eV; Zr $3d_{5/2}$: 179 eV[23]). This shift in binding energy corresponds to the reference values for ZrO_2[23] and thus indicates the presence of a native ZrO_2 film at the surface of the as-received Zr powder. Fig. 9(b) presents the binding energy spectra for Zr in the as-milled powders. Similarly, the two major peaks (184.6 and 182.2 eV) correspond to the ZrO_2 surface film present at the surface of the powder. A small bump was observed on the right side of the spectra and peak analysis has shown that this hump is composed of two reflections at 180.1 and 178.8 eV, respectively. These two peaks correspond to the Zr $3d_{3/2}$ and $3d_{5/2}$ binding energies of ZrB_2 reported in the literature, which are 180.9 and 178.6 eV, respectively.[24] This result indicates that,

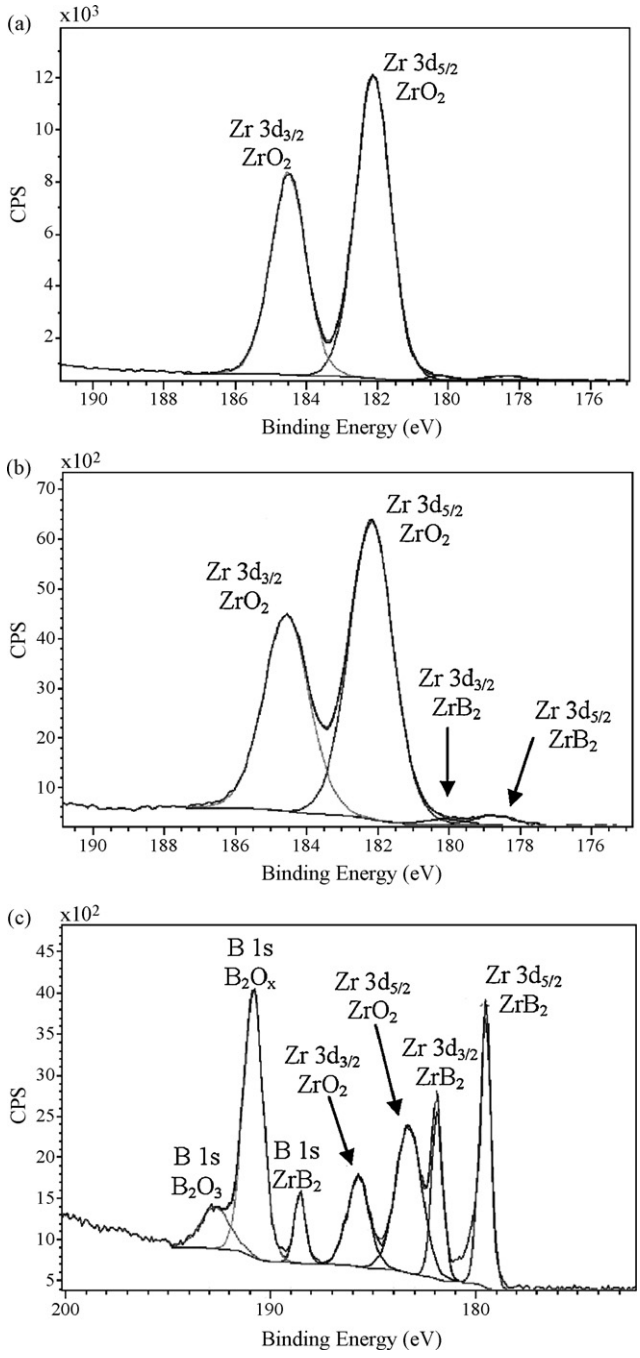

Fig. 9. XPS spectra of (a) starting Zr powders, (b) Zr–B mixture milled and (c) a hand-mixed sample sintered at 2200 °C.

despite the absence of X-ray diffraction peaks corresponding to ZrB_2, mechanical alloying occurred during the milling process. The volume fraction of ZrB_2 formed must be below 2 vol%, which is the nominal detection limit for the X-ray diffractometer used in this study. Fig. 9(c) shows the XPS spectrum for a hand mixed sample sintered at 2200 °C. The spectrum depicts binding energies corresponding to the ZrB_2 (Zr $3d_{3/2}$: 181.8 eV; Zr $3d_{5/2}$: 179.5 eV; B 1s: 188.5 eV) and the ZrO_2 surface film (Zr $3d_{3/2}$: 185.7 eV; Zr $3d_{5/2}$: 183.2 eV). In addition, a peak possessing an important shoulder is present on the high-energy portion and the peak fitting suggested the presence of B_2O_3 (B 1s: 192.7 eV)

and a non-stochiometric B_2O_x compound (B 1s: 190.8 eV). The binding energy for both types of B-based oxides are in agreement with literature values.[25–28] These results would suggests the presence of B oxides, which are known to reduce the densification and favor grain coarsening, explaining the results from the microstructure analysis. The presence of a non-stochiometric B_2O_x can be related to the evaporation of rapidly evolving gas species, such as BO, from $B_2O_{3(l)}$ at these temperatures This gas evolution was observed during sintering of B_4C by Dole et al.[29] Chamberlain et al.[14] reported that the presence of WC impurities from milling played a vital role in the removal of the surface oxide film. Despite all precautions taken to avoid contamination, oxygen contamination present as surface contamination of the starting Zr and most probably B powders, affected densification. The absence of oxygen detected in Fig. 9(b) would suggest a reaction between the Zr and the surface oxide of the B powder during milling. Since the milling procedure was carried out with a different milling media than WC, no mechanism for surface oxide removal was present, which can explained the significantly higher average grain size distribution when compared to other published works. The similarity in the densification rate and grain growth between the reactive hand mixed and the reactive Spex-milled methods suggested that the blending procedure studied in this work did not significantly contaminate the starting powder and, as demonstrated by the XPS results, the major source of oxygen contamination would come from the presence of surface oxide films at the surface of the starting powders.

4. Summary and conclusions

Bulk ZrB_2 ceramic was made by pressureless reactive sintering of elemental powder mixtures. XRD and microstructural analysis confirmed that no second phase was present after sintering. After reaction, the samples had relative densities ranging between 58 and 79%. Our results show that reaction by itself does not provide sufficient driving force to produce fully dense ZrB_2 from the elemental powders used here. Work by others[14,20,21] indicates that oxide impurities on grain boundaries slows the densification rate of ZrB_2. XPS analysis have shown that oxygen contamination is present at the surface of the starting material, which adversely affect the densification of the powders. The average grain size of the ZrB_2 ceramics increased when the heat treatment temperature is raised, from 8.5 to 13.2 to 23.5 μm for the hand mixed samples and from 4.6 to 13.0 to 34.9 μm for the Spex-milled samples.

References

1. Wang, C. R., Yang, J.-M. and Hoffman, W., Thermal stability of refractory carbide/boride composites. *Mater. Chem. Phys.*, 2002, **74**, 272–278.
2. Opeka, M. M., Talmy, I. G., Wuchina, E. J., Zaykoski, J. A. and Causey, S. J., Mechanical, thermal, and oxidation properties of refractory hafnium and zirconium compounds. *J. Eur. Ceram. Soc.*, 1999, **19**, 2405–2414.
3. Cutler, R. A., Engineering properties of borides, ceramic and glasses. In *Engineered Materials Handbook*, *vol. 4*, ed. S. J. Schneider. ASM International, 1992, pp. 787–803.
4. Chamberlain, A. L., Fahrenholtz, W. G., Hilmas, G. E. and Ellerby, D. T., High-strength zirconium diboride-based ceramics. *J. Am. Ceram. Soc.*, 2004, **87**(6), 1170–1172.
5. Fenter, J. R., Refractory diborides as engineering materials. *SAMPE Quart.*, 1971, **2**(3), 1–15.
6. Opeka, M. M., Talmy, I. G. and Zaykoski, J. A., Oxidation-based materials selection for 2000 °C + hypersonic aerosurfaces: theoretical considerations and historical experiences. *J. Mater. Sci.*, 2004, **39**, 5887–5904.
7. Parthasarathy, T. A., Rapp, R. A., Opeka, M. and Kerans, R. J., A model for the oxidation of ZrB_2, HfB_2 and TiB_2. *Acta Mater.*, 2007, **55**, 5999–6010.
8. Levine, S. R., Opila, E. J., Halbig, M. C., Kiser, J. D., Singh, M. and Salem, J. A., Evaluation of ultra-high temperature ceramics for aeropropulsion use. *J. Eur. Ceram. Soc.*, 2002, **22**, 2757–2767.
9. Monteverde, F., Bellosi, A. and Guicciardi, S., Processing and properties of zirconium diboride-based composites. *J. Eur. Ceram. Soc.*, 2002, **22**, 279–288.
10. Melendez-Martinez, J. J., Dominguez-Rodriguez, A., Monteverde, F., Melandri, C. and de Portu, G., Characterisation and high temperature mechanical properties of zirconium boride-based materials. *J. Eur. Ceram. Soc.*, 2002, **22**, 2543–2549.
11. Monteverde, F., Guicciardi, S. and Bellosi, A., Advances in microstructure and mechanical properties of zirconium diboride based ceramics. *Mater. Sci. Eng. A*, 2003, **346**, 310–319.
12. Woo, S.-K., Han, I.-S., Kim, H.-S., Kang, E.-S., Yang, J.-H. and Kim, C.-H., Sintering of zirconium diboride through Fe-based liquid phase. *J. Kor. Ceram. Soc.*, 1996, **33**(3), 259–268.
13. Telle, R., Sigl, L. S. and Takagi, K., Boride-based hard materials. In *Handbook of Ceramic Hard Materials*, *vol. 2*, ed. R. Riedel. Wiley-VCH, Weinheim, 2000, pp. 802–945.
14. Chamberlain, A. L., Fahrenholtz, W. G. and Hilmas, G. E., Pressureless sintering of zirconium diboride. *J. Am. Ceram. Soc.*, 2006, **89**(2), 450–456.
15. Fahrenholtz, W. G., Reactive processing in ceramic-based systems. *Int. J. Appl. Ceram. Technol.*, 2006, **3**, 1–12.
16. Chamberlain, A. L., Fahrenholtz, W. G. and Hilmas, G. E., Low-temperature densification of zirconium diboride ceramics by reactive hot pressing. *J. Am. Ceram. Soc.*, 2006, **89**(12), 3638–3645.
17. Monteverde, F., Progress in the fabrication of ultra-high-temperature ceramics: "in situ" synthesis, microstructure and properties of a reactive hot-pressed HfB_2–SiC composite. *Comp. Sci. Technol.*, 2005, **65**(11–12), 1869–1879.
18. Cullity, B. D., *Elements of X-ray Diffraction* (*2nd ed.*). Addison Wesley, 1978, pp. 409–411.
19. Alfa Aesar, supplier data.
20. Baik, S. and Becher, P. F., Effect of oxygen contamination on densification of TiB_2. *J. Am. Ceram. Soc.*, 1987, **70**(8), 527–530.
21. Lee, H. and Speyer, R. F., Pressureless sintering of boron carbide. *J. Am. Ceram. Soc.*, 2003, **86**(9), 1468–1473.
22. Fahrenholtz, W. G., The ZrB_2 volatility diagram. *J. Am. Ceram. Soc.*, 2005, **88**(12), 3509–3512.
23. *Handbook of X-ray Photoelectron Spectroscopy*. PerkinElmer Corporation, 1992, pp. 108–109.
24. *Standard Reference Database 20, NIST X-Ray Photoelectron Spectroscopy Database*. National Institute of Standards and Technology, US Department of Commerce.
25. *Handbook of X-ray Photoelectron Spectroscopy*. PerkinElmer Corporation, 1992, pp. 38–39.
26. Brainard, W. A. and Wheeler, A. D. R., XPS study of the adherence of refractory carbide, silicide and boride RF-sputtered wear-resistant coatings. *J. Vac. Sci. Technol.*, 1978, **15**(6), 1800–1805.
27. Schreifels, J. A., Maybury, P. C. and Swartz, W. E., X-ray photoelectron spectroscopy of nickel boride catalysts: correlation of surface states with reaction products in the hydrogenation of acrylonitrile. *J. Catal.*, 1980, **65**, 195–206.
28. Joyner, D. J. and Hercules, D. M., Chemical bonding and electronic structure of BO, HBO, and BN: an ESCA, Auger, SIMS, and SXS study. *J. Chem. Phys.*, 1980, **72**, 1095–1108.
29. Dole, S. L., Prochazka, S. and Doremus, R. H., Microstructural coarsening during sintering of boron carbide. *J. Am. Ceram. Soc.*, 1985, **68**(9), C-235–C-236.